3-D wavefront-oriented ray tracing: Estimation of traveltimes within cells

Radu Coman and Dirk Gajewski

email: *coman@dkrz.de*
keywords: *traveltimes, ray tracing, 3D*

ABSTRACT

Wavefront construction (WFC) methods permit the computation of multi-valued traveltimes for Kirchhoff migration. We present two approaches which increase the efficiency and accuracy of 3-D WFC methods. First, we apply three criteria for the insertion of new rays. In addition to the standard distance criterion we evaluate the possible crossing of rays, and introduce a criterion based on the difference in wavefront curvature between adjacent rays. Second, for the estimation of traveltimes within cells, we suggest a distance-weighted averaging of extrapolated traveltimes. The traveltimes are extrapolated under consideration of the wavefront curvature. Examples illustrate the high accuracy of the method.

INTRODUCTION

During the last years several papers have shown the importance of multivalued traveltime tables for the quality of migrated prestack Kirchhoff depth images. Multivalued traveltime tables are usually computed by WFC methods (Figure 1). In these methods adjacent rays are grouped into ray tubes, the ray density of the ray field is checked at wavefronts, and if necessary, new rays are inserted. The wavefront-oriented ray-tracing (WRT) technique (Coman and Gajewski, 2001) belongs to the larger group of WFC methods.

Usually in WFC methods, a new ray is inserted by interpolation on the wavefront between two adjacent rays (parent rays). To avoid interpolation, the WRT technique inserts a new ray by tracing it from the source. The accuracy of an interpolated ray is always less than the accuracy of the parent rays, while the accuracy of a traced ray is the same as the accuracy of the parent rays. Moreover, the accuracy of the ray inserted by tracing does not depend on the distance between the parent rays. The insertion of a new ray by tracing it from the source leads to higher accuracy and permits a lower ray density than the insertion by interpolation.

The WFC methods start with few rays which are propagated stepwise through the velocity model. A new wavefront is constructed from the old one by propagating the ray field with a constant traveltime step (*time step of wavefronts*). After the construction of a new wavefront, the traveltimes are estimated in the region between this wavefront and the previous one.

In the following sections, we present a new approach for the estimation of traveltimes within cells and a new set of criteria for the insertion of new rays. We implement both innovations in the WRT technique.

ESTIMATION OF TRAVELTIMES WITHIN CELLS

The ray tracing procedure computes the traveltimes at nodes, but for Kirchhoff depth migration the traveltimes are needed on a rectangular grid. The node-traveltimes are used to estimate the gridpoint-traveltimes. The estimation is carried out within cells. Figure 1 shows a 2-D sketch for simplicity. In 3-D, a cell is defined by six nodes (Figure 3). These nodes are the intersection of three adjacent rays and two adjacent wavefronts.

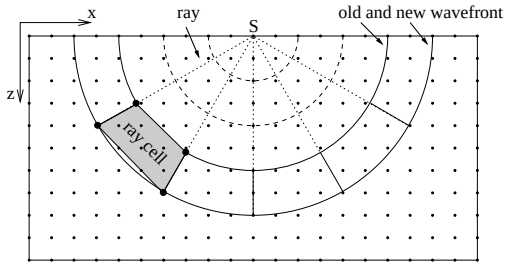

Figure 1: Graphical description of a 2-D WFC method. The traveltimes at nodes (large dots) are computed by ray tracing. The traveltimes at gridpoints (small dots) are estimated within a ray cell. Point S denotes the source point.

For the estimation of traveltimes within cells, Vinje et al. (1996) project the gridpoint on the old wavefront (for the old wavefront see Figure 1) and trace a ray back to the gridpoint. Lucio et al. (1996) split the cell into three tetrahedra and perform linear interpolation within the tetrahedra, while Bulant and Klimeš (1999) suggested a bicubic interpolation of traveltimes.

In this paper, we propose a distance-weighted averaging of extrapolated traveltimes. The extrapolation is performed from nodes to gridpoints under consideration of the wavefront curvature. The traveltimes are estimated and stored on a coarse grid, while the interpolation from the coarse grid to the fine migration grid is performed during the migration process (e.g., Vanelle and Gajewski, 2002). Our procedure for the estimation of traveltimes within cells can be split in four steps:

1. Estimation of the wavefront curvature
2. Decision whether a gridpoint belongs to the cell
3. Extrapolation of traveltimes
4. Distance-weighted averaging of extrapolated traveltimes

At a given node, e.g., node A_1 (Figure 3), the two principal wavefront curvatures are usually computed by dynamic ray tracing. Because the WRT technique does not apply dynamic ray tracing, we approximate the wavefront curvature using the sphere connecting the nodes A_1 and B_1 or A_1 and C_1 (Figure 3). Figure 2 illustrates the estimation of the wavefront curvature using the segment A_1B_1. For this estimation we use the position of the two nodes and the slowness vector at node A_1 to construct a sphere. We approximate the radius of the wavefront curvature at node A_1 by the radius of the sphere connecting A_1B_1. The same procedure is used for A_1C_1, i.e., two wavefront curvatures at point A_1 are obtained.

The second step is performed for each gridpoint within the rectangular box which bounds the cell. To determine whether a gridpoint is within a cell, we split the cell into three tetrahedra and use the approach proposed by Lucio et al. (1996). A slight modification of this approach permits the computation of the distances of the gridpoint to the sides of the tetrahedra. These distances are used for the computation of distance-weights. The last two steps are performed only for gridpoints within the cell.

We have mentioned above that at each node we know two wavefront curvatures. We extrapolate the traveltime from the node to a gridpoint considering each curvature separately. Because a cell is defined by six nodes, we have twelve extrapolated traveltimes at the gridpoint.

The traveltime t_G at gridpoint G (Figure 3) is estimated by a weighted average of the extrapolated traveltimes:

$$t_G = w_{a_1\beta} t_{a_1\beta} + w_{a_1\gamma} t_{a_1\gamma} + w_{b_1\alpha} t_{b_1\alpha} + \ldots,$$

where $t_{a_1\beta}$ is the extrapolated traveltime from node A_1 to gridpoint G using the wavefront curvature for the segment A_1C_1. The weight function $w_{a_1\beta}$ for the extrapolated traveltime $t_{a_1\beta}$ satisfy the relation

$$w_{a_1\beta} \sim \left(\frac{1}{d_1}\frac{1}{d_a}\frac{1}{d_\beta}\right)^2,$$

where the meaning of the distances d_1, d_a, d_β is shown in (Figure 3). The relations for other distance weights are similar.

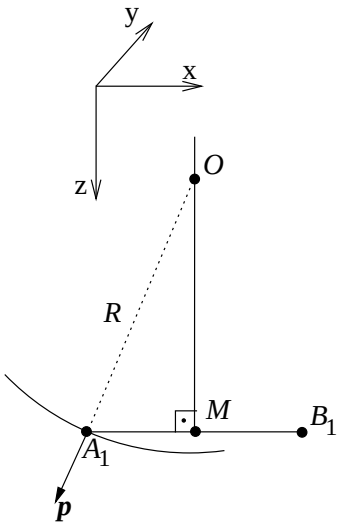

Figure 2: Approximation of the wavefront curvature at node A_1 using the segment A_1B_1. The radius of the wavefront curvature is approximated by the distance $|\overline{OA}|$. Point M is the midpoint of the segment $\overline{A_1B_1}$. Point O is obtained by the intersection of the continuation of the slowness vector $\mathbf{p}$ at A_1 with the plane normal to the segment $\overline{A_1B_1}$ at M.

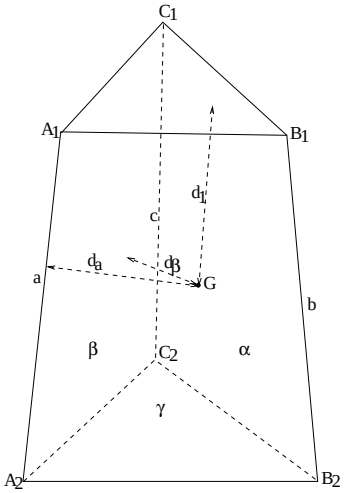

Figure 3: 3-D ray cell and the distances which are used for the computation of the distance weight $w_{a_1\beta}$. d_1 is the distance between gridpoint G and the upper triangular side, d_a is the distance between G and the ray segment A_1A_2, and d_β is the distance between G and the side β.

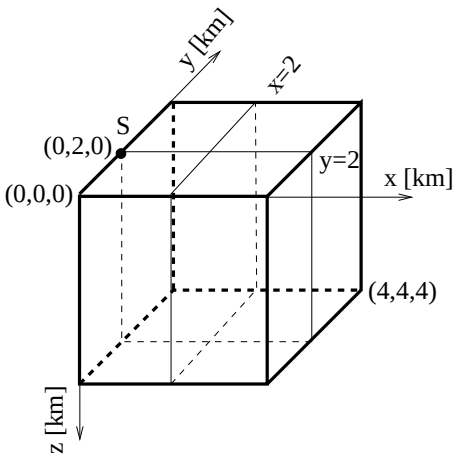

Figure 4: The geometry of the model is a cube with the side length of 4 km. The source S is located at the coordinates (0 km, 2 km, 0 km). The results of the computations are shown for two vertical slices at y=2 km, respectively at x=2 km.

CRITERIA FOR INSERTION OF NEW RAYS

We insert a new ray between two adjacent rays if one of the following criteria is satisfied: (1) the distance between the adjacent nodes exceeds a predefined node-distance threshold; (2) the difference in wavefront curvature between the rays exceeds a predefined threshold (time-difference threshold, see below).

Note that we prefer to express the difference in wavefront curvature in time units (milliseconds). For this reason we divide the difference between the radii of curvature by the velocity at the midpoint between the adjacent nodes.

The first insertion criterion is used in most WFC methods (e.g., Sun, 1992; Vinje et al., 1996; Ettrich and Gajewski, 1996; Coman and Gajewski, 2001). The second insertion criterion is new and replaces the insertion criterion which uses the difference in direction between adjacent rays. Using the difference in wavefront curvature as an insertion criterion permits a better control of the accuracy of the traveltime estimation within ray cells.

NUMERICAL EXAMPLES

To show the accuracy of the distance-weighted averaging of extrapolated traveltimes, we use two models which permit analytical computation of traveltimes. The first example is a homogeneous velocity model, the second one is a constant velocity gradient model. The geometry of the model in both cases is the same (Figure 4). The velocity in the homogeneous model is 2000 m/s. The velocity distribution in the constant velocity gradient model is given by $v(z)$ =2000 [m/s]+0.5 [1/s]z, where $v(z)$ is the velocity at depth z. We show the results for two vertical slices at $y = 2$ km, and at $x = 2$ km respectively (Figure 4).

In the first example (homogeneous model), we compare the distance-weighted averaging of extrapolated traveltimes to the linear interpolation between plane triangular sides. These sides approximate the wavefronts. For the propagation of the wavefront in the WRT technique, we use a time step of wavefronts of 0.1 s. A new ray is inserted if the distance between adjacent rays gets larger than 500 m.

The wavefronts constructed from analytical traveltimes are shown in Figure 5a and 5b. The traveltime errors due to the linear interpolation are shown in Figure 5c and 5d, and the errors due to the distance-weighted averaging of extrapolated traveltimes are shown in Figure 5e and 5f. Note that even in this homogeneous velocity model, the linear interpolation leads to errors up to 10 ms. The traveltime errors when using the distance-weighted averaging of extrapolated traveltimes are much smaller (less than 10^{-3} ms).

In the second example (constant velocity gradient model) we show the influence of the distance dependent weights on the accuracy of computed traveltimes. To analyze this influence we compute the traveltimes with and without distance weights. For the computation of traveltimes with the WRT technique, we use a time step of wavefronts of 70 ms, a node-distance threshold of 300 m and a time-difference threshold of

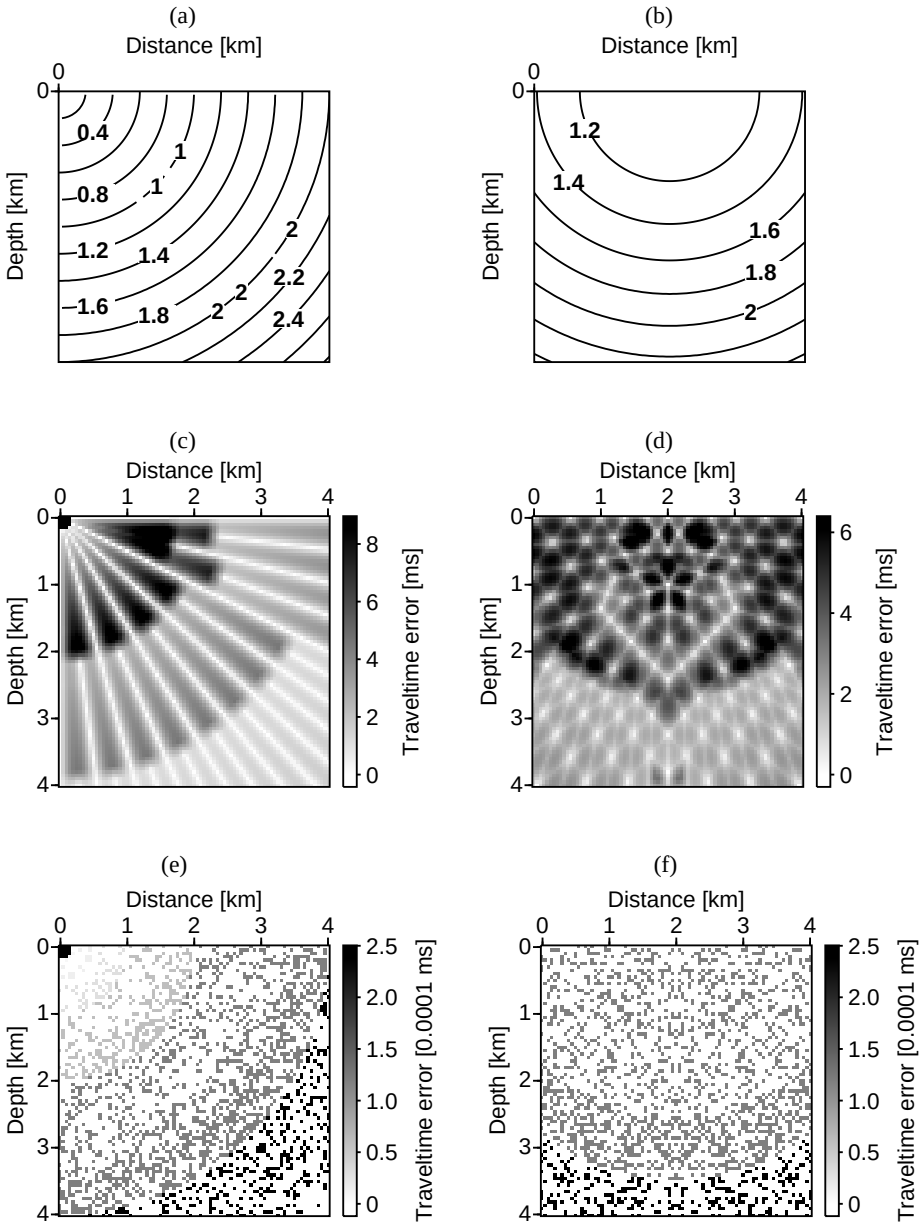

Figure 5: Results of the computation in the homogeneous velocity model in two vertical slices: (a), (c) and (e) for the vertical slice at $y = 2$ km; (b), (d) and (f) for the vertical slice at $x = 2$ km. (a) and (b) Wavefronts constructed from analytically computed traveltimes. (c) and (d) Traveltime errors due to the linear interpolation. (e) and (f) Traveltime errors due to the distance-weighted averaging of extrapolated traveltimes. Note the different error scales.

1 ms.

The wavefronts constructed from analytical traveltimes are shown in Figure 6a and 6b. The traveltime errors due to the the non-weighted averaging of extrapolated traveltimes (Figure 6c and 6d) are small along the rays and along the wavefronts, but the errors are large within the cells. The errors can be substantially reduced when using the distance dependent weights (Figure 6e and 6f). In this example, the maximal traveltime error has been reduced by a factor 20 (from 0.3 ms to 0.015 ms)

The distribution of the errors for traveltimes computed by the distance-weighted averaging of extrapolated traveltimes in the vertical slice defined by $y = 2$ km (Figure 6e) leads to two observations. First, the traveltime error increases with the increase of the difference in the wavefront curvature between adjacent ray. In the second numerical example, this difference is large at small traveltimes. In these regions the traveltime error is controlled by the time-difference threshold. Second, the insertion of a new ray reduces the traveltime errors. Note that this is true only if the new ray is traced from the source.

CONCLUSIONS

The insertion of a new ray by tracing it directly from the source increases the accuracy of traveltimes and permits a lower ray density, i.e., larger cells, than in other WFC methods. For an efficient estimation of traveltimes within large cells, we have presented the distance-weighted averaging of extrapolated traveltimes. The extrapolation of traveltimes uses the wavefront curvature. We have shown that not only the extrapolation of traveltimes but also the distance dependent weights are important for the accuracy of the traveltime estimation. Because the accuracy of the estimation depends on the difference in wavefront curvature, we use this difference as an insertion criterion for new rays. This criterion permits a better control of the traveltime errors and of the ray density.

ACKNOWLEDGEMENTS

This work was partially supported by the sponsors of the *Wave Inversion Technology (WIT) Consortium*, Karlsruhe, Germany, and the German Israeli Foundation (I-524-018.08\97). Continuous discussions with the members of the Applied Geophysics Group, Hamburg are appreciated.

REFERENCES

Bulant, P. and Klimeš, L. (1999). Interpolation of ray theory traveltimes within ray cells. *Geophys. J. Int.*, 139:273–282.

Coman, R. and Gajewski, D. (2001). Estimation of multivalued arrivals in 3-D models using wavefront ray tracing. In *Expanded Abstracts*, pages 1265–1268. Soc. Expl. Geophys.

Ettrich, N. and Gajewski, D. (1996). Wavefront construction in smooth media for pre-stack depth migration. *Pure Appl. Geophys.*, 148:481–502.

Lucio, P., Lambaré, G., and Hanyga, A. (1996). 3D multivalued travel time and amplitude maps. *Pure Appl. Geophys.*, 148:449–479.

Sun, Y. (1992). Computation of 2D multiple arrival travel time fields by an interpolative shooting method. In *Expanded Abstracts*, pages 1320–1323. Soc. Expl. Geophys. Tulsa, OK.

Vanelle, C. and Gajewski, D. (2002). Second-order interpolation of traveltimes. *Geophysical Prospecting*, 50:73–83.

Vinje, V., Iversen, E., Åstebøl, K., and Gjøystdal, H. (1996). Estimation of multivalued arrivals in 3D models using wavefront construction–Part I. *Geophysical Prospecting*, 44:819–842.

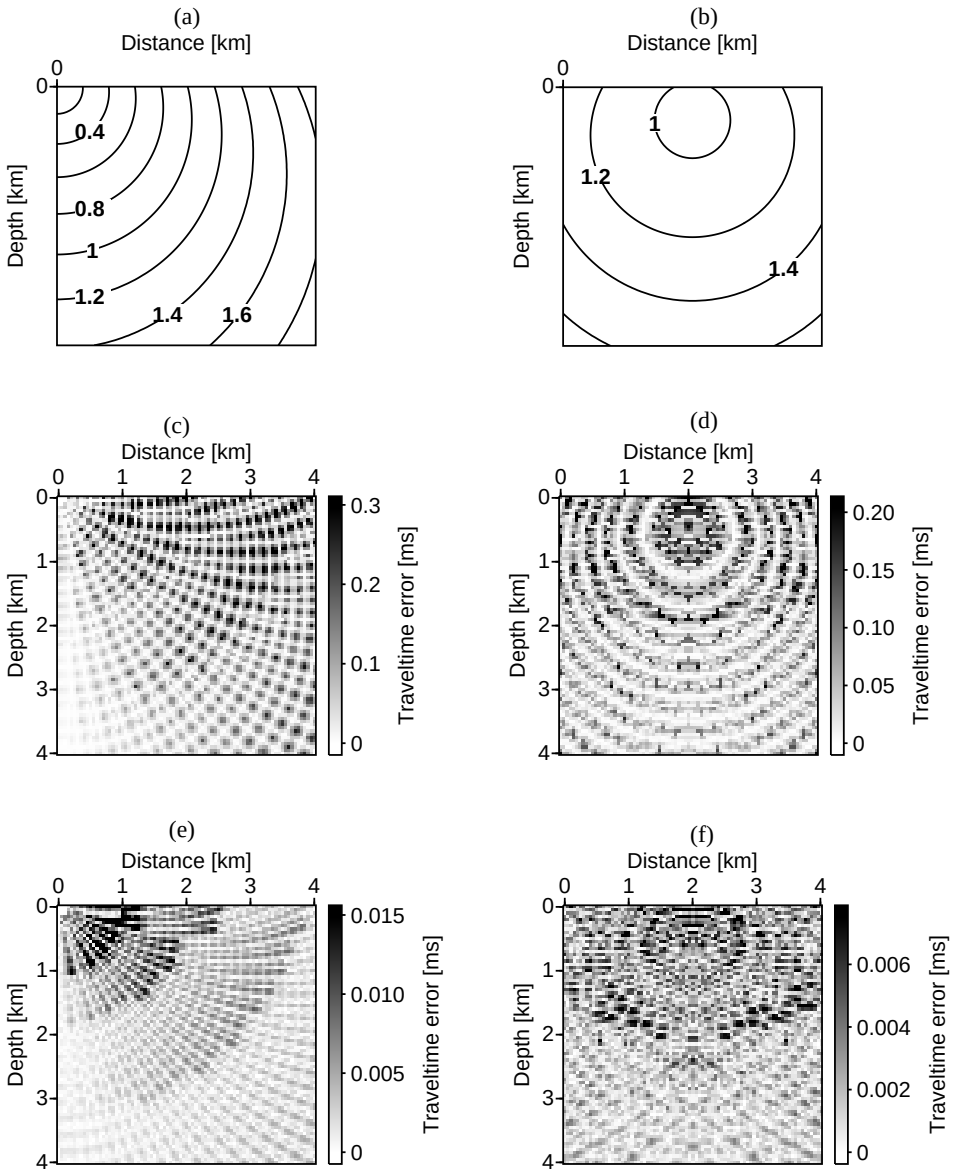

Figure 6: Results of the computation in the constant velocity gradient model in two vertical slices: (a), (c) and (e) for the vertical slice at $y = 2$ km; (b), (d) and (f) for the vertical slice at $x = 2$ km. (a) and (b) Wavefronts constructed from analytically computed traveltimes. (c) and (d) Traveltime errors due to the non-weighted averaging of extrapolated traveltimes. (e) and (f) Traveltime errors due to the distance-weighted averaging of extrapolated traveltimes.